GEOPHYSICS

Optical interferometry–based array of seafloor environmental sensors using a transoceanic submarine cable

G. Marra[1]*, D. M. Fairweather[2], V. Kamalov[3], P. Gaynor[1], M. Cantono[3], S. Mulholland[1], B. Baptie[4], J. C. Castellanos[3], G. Vagenas[1], J.-O. Gaudron[1], J. Kronjäger[1], I. R. Hill[1], M. Schioppo[1], I. Barbeito Edreira[1], K. A. Burrows[1], C. Clivati[5], D. Calonico[5], A. Curtis[2]

Optical fiber–based sensing technology can drastically improve Earth observations by enabling the use of existing submarine communication cables as seafloor sensors. Previous interferometric and polarization-based techniques demonstrated environmental sensing over cable lengths up to 10,500 kilometers. However, measurements were limited to the integrated changes over the entire length of the cable. We demonstrate the detection of earthquakes and ocean signals on individual spans between repeaters of a 5860-kilometer-long transatlantic cable rather than the whole cable. By applying this technique to the existing undersea communication cables, which have a repeater-to-repeater span length of 45 to 90 kilometers, the largely unmonitored ocean floor could be instrumented with thousands of permanent real-time environmental sensors without changes to the underwater infrastructure.

Despite substantial expansion of sensing capabilities, seas and oceans remain mostly unmonitored, limiting our understanding of Earth's structure and its dynamic behavior. However, research on techniques exploiting the sensitivity of optical fiber to environmental perturbations over the past few years has shown that the existing network of submarine cables could potentially be used as seafloor sensors. While backscattering-based techniques, such as distributed acoustic sensing (DAS), provide high sensitivity and spatial resolution, such approaches are currently limited to coastal areas up to 100 km from the shore owing to signal attenuation (*1*–*4*). Previously, we showed that optical interferometric techniques, which detect optical phase changes, provide a solution for monitoring over much longer distances than the working range of DAS, but at the expense of a lower spatial resolution (*5*). More recently, Zhan *et al*. demonstrated that polarization of light can also be used for environmental sensing over submarine cables up to 10,500 km in length (*6*). However, in both techniques, the measured quantity is the cumulative phase or polarization change over the entire length of the optical fiber cable. Although the detection of earthquakes and ocean waves was successfully demonstrated, measuring the integrated perturbations over the entire cable length has two major limitations. First, the measurement noise floor is set by the background environmental noise integrated over the entire cable length. This limits the detection of smaller-sized earthquakes and other environmental signals of interest. Second, because the cable acts as a single sensor, signals from multiple cables are required to triangulate the location of sources, such as earthquake epicenters (*5*).

Our work overcomes the first limitation and substantially improves on the second by using an optical technique that enables the measurement of environmentally induced optical phase changes over individual sections of the submarine cable rather than its entire length. In doing so, we demonstrate the detection of earthquakes, microseisms, and ocean currents spatially resolved at several locations along the cable. We show that the substantially higher sensitivity achieved by this interferometry-based technique enables the detection of signals that could not be observed when measuring the cumulative optical perturbation across the entire cable. Lastly, we show that, by performing spanwise measurements, a single cable is sufficient to identify the epicentral region of a teleseismic earthquake.

The cable sections correspond to one or more spans between the repeaters used for the amplification of the optical signal along the cable. The technique we used allows for the environmentally induced optical perturbations in each cable section to be measured independently, effectively converting a submarine cable into an array of fiber-based sensors. The number of sensors can be as high as the number of repeater-to-repeater cable spans. For an intercontinental link, such as the one we used, the number of spans can exceed 100. The technique we present has the potential to transform our Earth-monitoring capabilities, as the currently greatly undersampled seafloor could be instrumented with thousands of interferometry-based sensors without modifying the existing submarine telecommunication infrastructure. Crucially, although in our work we used a research-grade ultrastable laser, we show that more compact and lower cost narrow-linewidth telecommunications lasers could also be used with limited or no loss of sensitivity. This feature makes our technique highly scalable toward potential conversion of the existing subsea cable infrastructure into a global network of environmental sensors.

We achieved an array of sensing elements by exploiting the architecture of repeaters in modern submarine cables. These repeaters often include a high-loss loop back (HLLB) path that enables a small fraction of the transmitted light to be returned to the transmitting end via the second fiber of the fiber pair (Fig. 1). On many cables, the return path is implemented by using fiber Bragg gratings (FBGs), acting as narrow-band reflectors (fig. S1A). These return paths are used by the cable operator to periodically check the health of the optical amplifiers (*7*). These checks are typically performed on a schedule or if there is a malfunction, leaving these channels unused most of the time. By injecting infrared light from an ultrastable laser source and performing high-precision interferometric measurements of the signal returned by the HLLBs, we extracted the round-trip (loop-back) accumulated optical phase changes in the fiber between the transmitter end of the cable and the chosen repeaters. To localize the perturbations to cable sections between two or multiple repeaters, we computed the difference between loop-back signals. As the wavelength of the FBG reflectors is the same for all HLLBs, we used an optical technique called optical frequency domain reflectometry (*8*), whereby the frequency of the light source is swept such that the loop-back signal from each repeater can be separated in the frequency domain. This technique is used in some Rayleigh scattering–based fiber sensing applications (*9*). However, in our test, we did not use the scattered light from the fiber inhomogeneities but rather the signal returned by the FBG-based reflector in the HLLBs. This resulted in a returned signal that was orders of magnitude higher in amplitude than from back-scattering. The frequency-swept laser light was injected into the forward path of the submarine cable. The light returned at the transmitter, which consisted of the overlap of the returned light from each repeater, was combined on a photodetector with the output of the swept laser. Here, a series of radio frequency signals was obtained, where each frequency identifies a different repeater with frequency proportional to the round-trip time (fig. S2). Each loop-back beat note was spectrally filtered and its phase, relative to that of the local laser source, was measured with a phase meter.

[1]National Physical Laboratory (NPL), Teddington, UK. [2]School of GeoSciences, University of Edinburgh, Edinburgh, UK. [3]Google LLC, Mountain View, CA, USA. [4]British Geological Survey, Edinburgh, UK. [5]Istituto Nazionale di Ricerca Metrologica (INRIM), Turin, Italy.
*Corresponding author. Email: giuseppe.marra@npl.co.uk

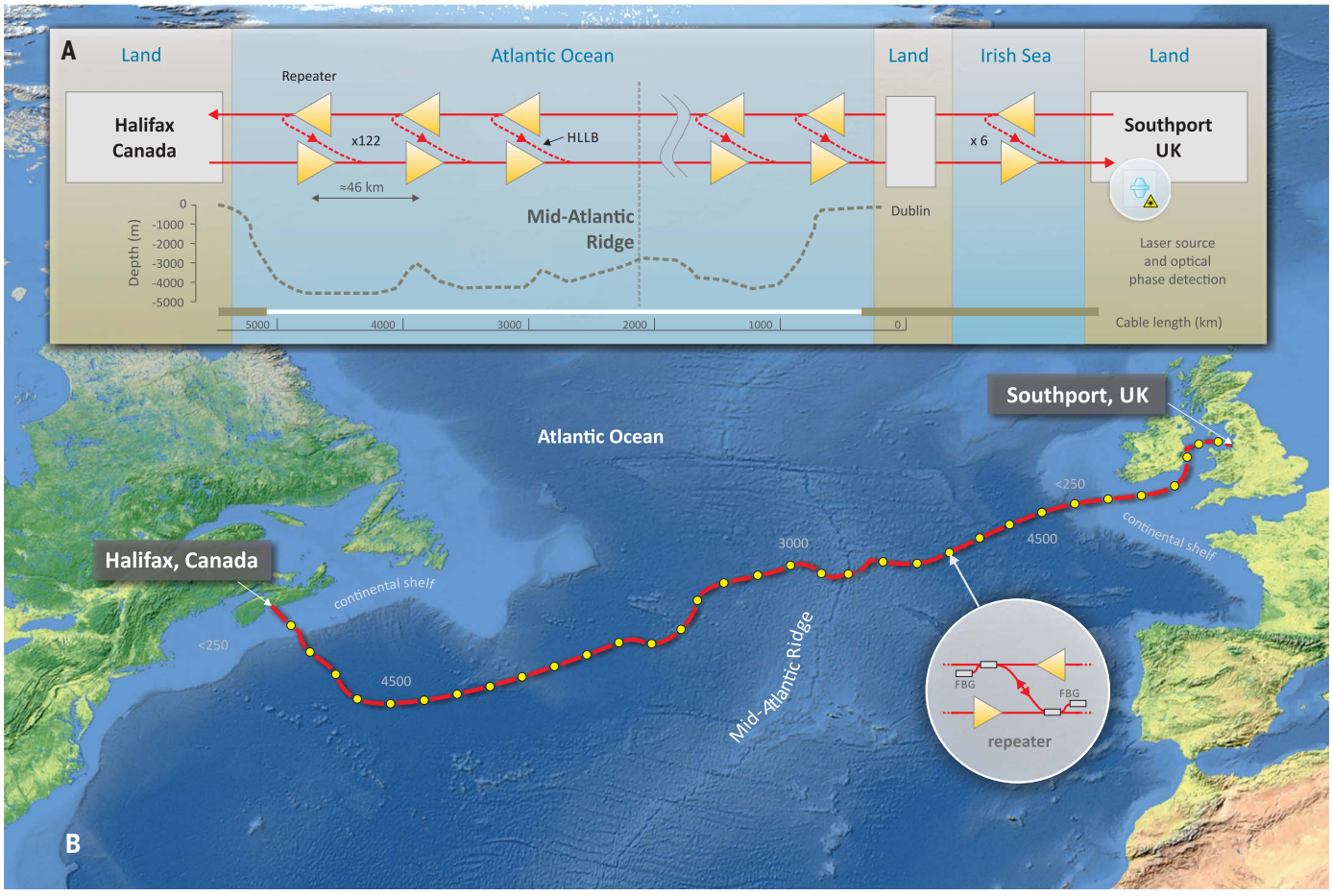

Fig. 1. Map and details of the UK-Canada submarine link. (**A**) Illustration of the high-loss loop back (HLLB) architecture and cable bathymetry. (**B**) Map of the UK-Canada submarine cable. The actual number of repeaters (128) was reduced in the figure for illustration purposes. Each repeater has a pair of fiber Bragg grating (FBG) reflectors.

We tested this technique on a 5860-km-long intercontinental submarine optical fiber link between the UK and Canada. The link consists of two cables: a 248-km-long cable from Southport, UK, to Dublin, Ireland, and a 5612-km-long cable from Dublin to Halifax, Canada. A total of 128 optical repeaters are installed on the link, and the average span between them is 46 km. Our experimental setup allowed us to simultaneously measure loop-back signals from up to 12 repeaters at a time, which could be selected. The hardware upgrades required to extend the monitoring capability to the full number of spans between repeaters are shown in fig. S3. Because of temperature-induced polarization changes in the cable, the signal-to-noise ratio (SNR) of some of the available loop-back signals could temporarily become insufficient for the frequency counter to perform a correct measurement. In our tests, on average, seven to nine loop-back signals exhibited sufficient SNR. Moreover, the SNR of the returned signal degraded because of the accumulation of amplified spontaneous emission noise of the optical amplifiers for repeaters increasingly distant from the transmitting end. In our tests, we obtained signals with sufficient SNR from repeaters at a cable distance up to 3100 km. As this is more than half of the cable length, monitoring of all the submarine cable spans could be achieved by also measuring from the Canadian end. Both the polarization-induced degradation of the signal and the range of usable loop-back signals can be, respectively, eliminated and extended with further upgrades (*10*). We also successfully tested our technique while data traffic was present on other channels available in the fiber pair. This demonstrates the compatibility of our technique with standard optical communication technology, which is a crucial prerequisite for its wide application over the submarine telecommunication network.

We show the detection of two earthquakes on multiple submarine cable spans, the Northern Peru moment magnitude (M_w) 7.5 earthquake (28 November 2021) and the Flores Sea M_w 7.3 earthquake (14 December 2021), respectively (Fig. 2, A and B). We detected the Northern Peru earthquake on six of the nine sections of the cable being tested. We plotted a spectrogram and time series of the signals detected by three of these sections (Fig. 2A). The signals and location of the additional six spans are shown in fig. S4. The spectrograms display the temporal evolution of the power spectral density (PSD) of the frequency fluctuations of the optical signal, induced by environmental perturbations, over the cable section that is being measured. For all the data shown in this work, we choose to display the optical frequency deviation rather than phase deviation, as we experimentally find that this allows us to better visualize notable features in the detected signals. Several factors can contribute to the amplitude of the observed waveform, including the earthquake fault geometry, the three-dimensional heterogeneity of the seismic structure between the fault and cable, the coupling of the cable to the external environment, and the

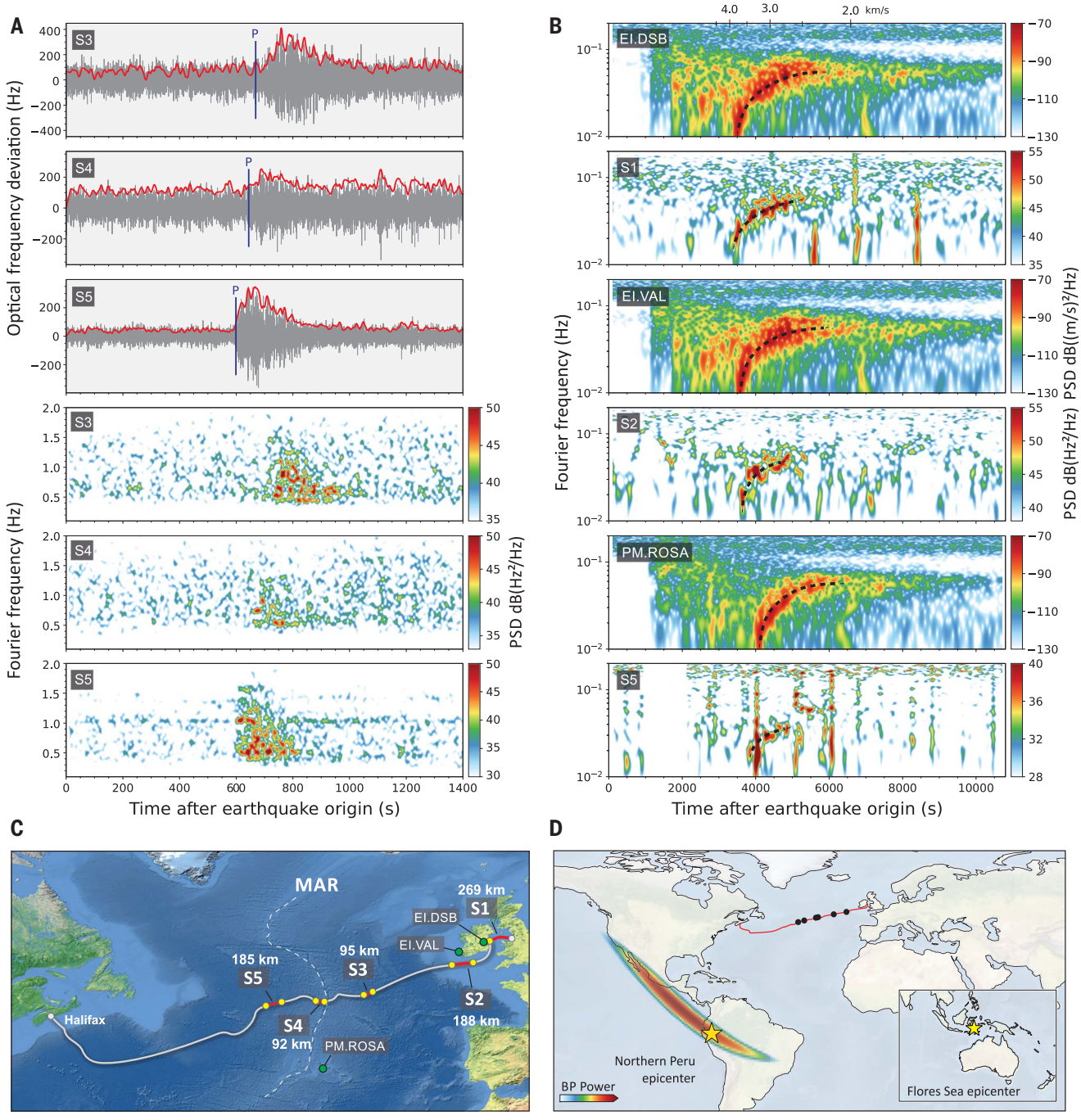

Fig. 2. Earthquake detections on submarine cable spans. (**A**) Time series and spectrograms of the optical frequency deviation induced by the Northern Peru earthquake detection. Vertical blue lines show the theoretical P wave arrival time. (**B**) Spectrograms of the Flores Sea earthquake detected by the cable sections and compared with their nearest seismic stations on land. The dashed black lines on the spectrograms track the surface wave group velocity dispersion. As a reference, we show the group velocity scale for station EI.DSB (Dublin, Ireland, Irish National Seismic Network). EI.VAL, Valentia, Ireland, Irish National Seismic Network; PM.ROSA, Rosais, Azores, Portugal, Portuguese National Seismic Network. (**C**) Map of the cable sections used for data displayed in (A) and (B) and location of the seismometers considered in (B). (**D**) Geographical area for the epicenter location for the Northern Peru earthquake, obtained by back-projection. The heatmap represents the probability of the epicenter location, with warm colors representing a higher probability. The stars indicate the event epicenters, as reported by the Global Centroid Moment Tensor earthquake catalog (*19*, *20*), and the black dots show the locations of the six cable sections used for the back-projection (*10*).

length of the fiber. Further tests on a larger number of spans and events will allow better characterization of the weight of each contribution. From the time lag between envelopes of the detected teleseismic P waves (Fig. 2A) and using a simple back-projection (BP) approach (*10*), we were able to resolve the epicentral location of the seismic event (Fig. 2D).

The Flores Sea earthquake was detected on five of the nine cable sections being tested (fig. S7). The spectrogram of the optical frequency deviations (Fig. 2B) induced by the seismic wave on the S1, S2, and S5 cable sections (Fig. 2C) is shown in comparison with the closest available seismic station on land.

Although the P wave arrival is not visible on the span data, the surface wave dispersion is clearly resolved and shows very good agreement with that measured by land seismometers. In addition to the measurements on separate sections of the cable, we also measured the optical frequency changes on the entire UK-Canada cable on a separate channel of the same fiber pair. We performed this measurement by connecting the fiber pair together at the Halifax end, such that we obtained a return signal in Southport after a 11,720-km-long round trip. We stress that in this arrangement the signal does not go through the HLLBs but forward-propagates for the entire length of the cable, as in our previous work (*5*). Whereas the surface wave of the Flores Sea earthquake was also visible in the full-cable measurement (fig. S7), the Northern Peru earthquake was not detected (fig. S4). This is because the detected surface waves from the Flores Sea signal had components between 0.01 and 0.1 Hz, which we measured to be a relatively low noise frequency range on the seafloor, whereas the detected body waves from the Northern Peru signal had components in the 0.1 to 5 Hz range, which is considerably noisier. The detection

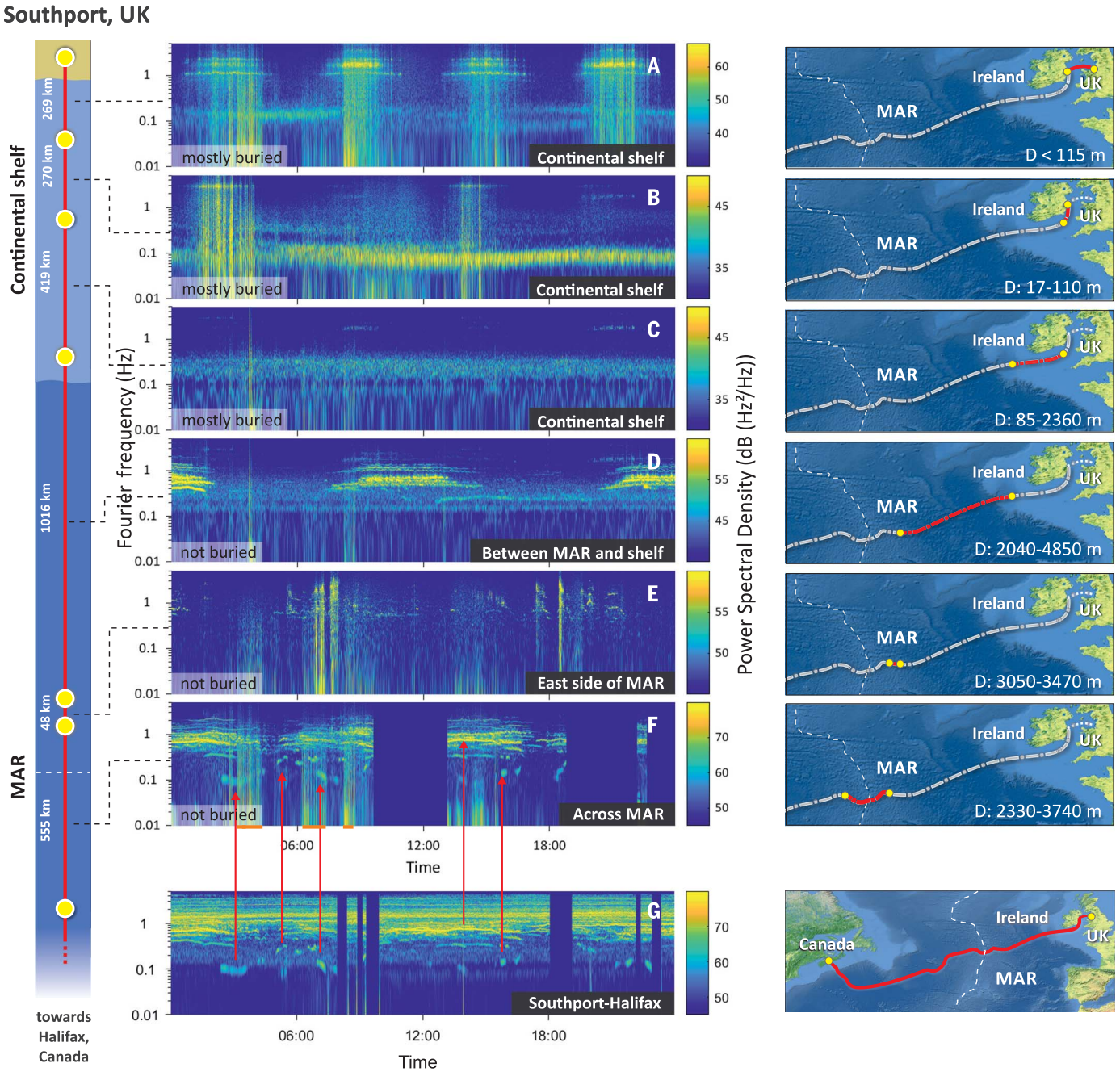

Fig. 3. Environmental noise detected by different sections of the trans-Atlantic cable. (**A** to **F**) Environmental noise detected on continental shelf, deep ocean, and Mid-Atlantic Ridge sections of the cable. (**G**) Environmental noise detected on the full link. Data with insufficient SNR was removed. The range of the color bar of each spectrogram is adjusted to best visualize the detected signals. The impulsive noise in the spectrograms corresponding to the time marked by the short horizontal orange lines at the bottom of (F) is due to glitches caused by temporary issue with the laser locking setup and not to environmental noise on the seafloor. D, depth.

of the Northern Peru earthquake therefore demonstrates the substantially better detection threshold achieved with spanwise measurements, as the background environmental noise on the other parts of the cable does not contribute to the measurement noise floor.

We show the spectrogram of the environmental noise measured by different sections of the intercontinental submarine cable from the cable landing station (CLS) in Southport to the Mid-Atlantic Ridge (MAR) on 21 October 2021 (Fig. 3). On the first 269-km cable section, which crosses the Irish Sea floor, we observed narrow-band components in the 1 to 5 Hz range that repeated approximately every 6 hours (Fig. 3A). This periodic pattern is synchronous with tidal currents in the Irish Sea, and their amplitude correlates well with the neap/spring cycle, as shown by a longer dataset in Fig. 4A. We speculate that the observed signals arise from "strumming" of exposed cable sections or pressure changes induced by the tidal currents. We also observed these periodic signals on the second section close to the southeastern coast of Ireland (Fig. 3B), although they were less pronounced, and a strong microseismic component in the 0.07 to 0.15 Hz range. The latter feature was likely caused by the coupling of ocean wave energy to the shallow seafloor.

On the cable section that extends from the Irish coast to the end of the continental shelf, where the bathymetry is consistently flat, we observed a drop in the environmental noise level of up to 30 dB (Fig. 3C and fig. S8). On the fourth section (Fig. 3D), extending from the end of the continental shelf to the MAR area, we detected excess noise between 0.5 and 1.5 Hz, this time with a 12-hour repeating pattern, which we attribute to tidal currents in the MAR area. We also observed a large increase in the detected noise as the cable approaches and crosses the MAR (Fig. 3, E and F). We attribute this to the interaction of ocean currents with the changing MAR bathymetry. Around this area, sea mounts rise from 3740 to 2330 m water depth, with the cable possibly being suspended between irregularities of the seafloor and thus more subject to current-induced movement. By comparing Fig. 3F and Fig. 3G, we can identify several features on the spectrogram of the integrated round-trip signal over the entire Halifax-Southport cable (Fig. 3G) on that of the cable section across the MAR (Fig. 3F), indicating that this area is a large contributor to the overall measured noise. We also observed a high level of correlation of the periodic signals observed on the shallow water sections of the cable with the tidal current velocity (Fig. 4A). We also found a high level of correlation between the signals in the 0.1 to 0.5 Hz range and the wave height measured at the M2 buoy in the Irish Sea (Fig. 4A). We identified Hurricane Larry to be the likely source of the dispersive microseism in the 0.05 to 0.1 Hz frequency range between 13 and 17 September (*10*). We show an 8-day-long dataset in late November 2021 (Fig. 4B), on

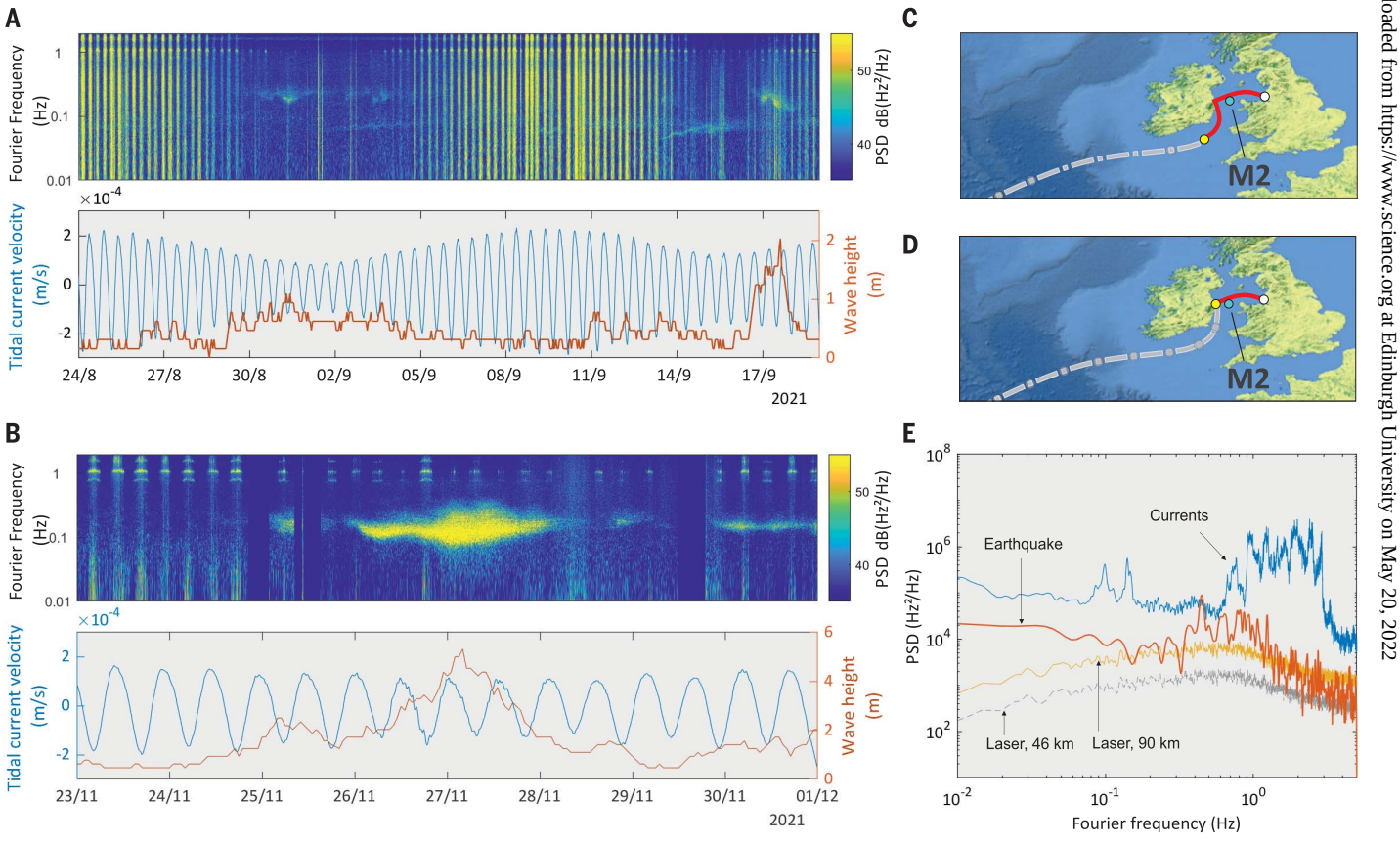

Fig. 4. Correlation of detected signals on cable spans with wave height and tidal currents. (**A**) Spectrogram of the frequency changes detected on the span shown in (C) compared with wave height measured at the M2 buoy in the Irish Sea and tidal current velocity measured by the Dublin Port tide gauge, showing a high degree of correlation. (**B**) Storm detected on the span shown in (D) in late November 2021 and correlation with water levels and tidal current velocity measured in the Irish Sea. (**C** and **D**) Maps of the cable sections used and M2 buoy. (**E**) Comparison between the power spectral density of environmental signals (earthquake and currents) and the calculated measurement noise floor that would be obtained if an off-the-shelf telecommunication narrow-linewidth laser, instead of research-grade laser, were used on a 46-km and 90-km span (*10*).

the cable section shown in Fig. 4D. During this time, an extratropical cyclone moved southward across the UK, and a resulting strong microseismic component was observed on the Southport-Dublin section of the cable. This correlates very well with the increase of average wave height measured at the M2 buoy.

Crucially, in contrast to previous optical interferometric tests, which required a research-grade ultrastable laser (*5*), the technique we have demonstrated here greatly relaxes the requirements on the laser source. Because the optical perturbations are measured over sections of the cable rather than the whole length, the requirement for the laser coherence length is scaled accordingly (*10*). For the submarine cable used in these tests, the coherence length requirement is reduced by approximately a factor of 129, equating to the number of ~46-km-long spans between repeaters and to the CLSs. Although in our experiment we still used a research-grade stabilized laser developed at NPL, we show that commercially available narrow-linewidth lasers could be used instead to detect most of the signals we have presented. An example is in the PSD of the M_w 7.5 Peru earthquake (Fig. 4E) detected on the 95-km-long S3 span of Fig. 2C. For comparison, the contribution of the laser instability of a narrow-linewidth telecommunication laser to the measurement noise floor over the same span length is displayed. We also show the PSD of the current-induced noise measured over the 92-km-long S4 span west of MAR, which is up to 30 dB above the expected laser contribution to the noise floor.

By enabling the use of commercially available telecommunication lasers, our technique could easily be scaled up and applied to a large number of cables in the existing submarine network. By converting submarine cables into arrays of environmental sensors, a large network of hundreds or thousands of permanent and real-time seafloor sensors could be implemented without modification of the existing subsea infrastructure. This has the potential to transform our understanding of both shallow and deep processes inside Earth. The ability to record seismic phases in the middle of ocean basins could enable the imaging of previously obscured structures such as mid-ocean ridges and oceanic fault zones, advancing our understanding of the processes that underlie the generation of oceanic crust (*11*) and the mechanisms by which oceanic plates are hydrated (*12*).

The cable sensitivity to water currents could be explored to improve our understanding of deepwater flows (thermohaline circulation), including the proposed slowing down of ocean currents due to rising global temperatures (*13*, *14*). Furthermore, the joint detection of deepwater currents and seafloor pressure changes caused by the passing of ocean waves implies strong potential for tsunami sensing (*15*, *16*). Lastly, while more research is needed to characterize long-term measurement drifts (*10*), the sensitivity of the optical cables to temperature could be explored for climate change research (*17*, *18*).

REFERENCES AND NOTES

1. E. F. Williams *et al*., *Nat. Commun.* **10**, 5778 (2019).
2. N. J. Lindsey, T. C. Dawe, J. B. Ajo-Franklin, *Science* **366**, 1103–1107 (2019).
3. Z. J. Spica *et al*., *Geophys. Res. Lett.* **47**, e2020GL088360 (2020).
4. E. F. Williams *et al*., *Lead. Edge* **40**, 576–583 (2021).
5. G. Marra *et al*., *Science* **361**, 486–490 (2018).
6. Z. Zhan *et al*., *Science* **371**, 931–936 (2021).
7. N. S. Bergano *et al*., in *Undersea Fiber Communication Systems*, J. Chesnoy, Ed. (Academic Press, ed. 2, 2016), pp. 427–430.
8. W. Eickhoff, R. Ulrich, *Appl. Phys. Lett.* **39**, 693–695 (1981).
9. Z. Ding *et al*., *Sensors* **18**, 1072 (2018).
10. Materials and methods are available as supplementary materials.
11. R. C. Searle, A. V. Bralee, *Geochem. Geophys. Geosyst.* **8**, Q05015 (2007).
12. C. M. Eakin, C. A. Rychert, N. Harmon, *J. Geophys. Res. Solid Earth* **123**, 1736–1751 (2018).
13. J. R. Toggweiler, R. M. Key, in *Encyclopedia of Ocean Sciences*, J. H. Steele, Ed. (Academic Press, 2001), pp. 2941–2947.
14. J. M. Gregory, R. Tailleux, *Clim. Dyn.* **37**, 893–914 (2011).
15. A. B. Rabinovich, M. C. Eblé, *Pure Appl. Geophys.* **172**, 3281–3312 (2015).
16. R. E. Thomson *et al*., *Geophys. Res. Lett.* **38**, L11701 (2011).
17. W. Wu, Z. Zhan, S. Peng, S. Ni, J. Callies, *Science* **369**, 1510–1515 (2020).
18. C. S. Meinen, R. C. Perez, S. Dong, A. R. Piola, E. Campos, *Geophys. Res. Lett.* **47**, (2020).
19. A. M. Dziewonski, T.-A. Chou, J. H. Woodhouse, *J. Geophys. Res.* **86**, 2825–2852 (1981).
20. G. Ekström, M. Nettles, A. M. Dziewonski, *Phys. Earth Planet. Inter.* **200–201**, 1–9 (2012).
21. G. Marra *et al*., Interferometric array data for UK-Canada seafloor cable v1.0 Zenodo (2022); https://doi.org/10.5281/zenodo.6405431.

ACKNOWLEDGMENTS

We thank J. Tunesi and R. M. Godun (NPL) for careful reading of the manuscript and S. Robinson for useful discussions. We thank the NPL IT team for help setting up the NPL-Southport remote access capabilities. We thank EXA Infrastructure for providing access to the submarine cable. We thank U. Hölzle, B. Koley, and V. Vusirikala (Google LLC) for support and discussions, and D. Lloyd, M. Cox, T. Dickenson, M. Wildman, L. Taylor, and A. Walsh (EXA Infrastructure) and T. Aydin (Google LLC) for support on setting up the experiments on the UK-Canada cable. **Funding:** NPL: This work was supported by an ISCF Metrology Fellowship grant and as part of the National Measurement System Programme provided by the UK government's Department for Business, Energy and Industrial Strategy (BEIS), and by an Award from the National Physical Laboratory's Directors' Science and Engineering Fund. University of Edinburgh: This work was supported by the Engineering and Physical Sciences Research Council Doctoral Training Project EP/T517884/1. British Geological Survey: This work was funded by the Natural Environment Research Council (NERC). INRIM: This project received funding from the European Union's Horizon 2020 research and innovation programme under grant 951886 (CLONETS-DS). **Author contributions:** G.M., V.K., M.C., and D.C. planned and designed the work. G.M., S.M., and P.G. designed the experimental setup. P.G., S.M., G.V., J.-O.G., I.B.E., M.S., I.R.H., and G.M. built the experimental setup. G.M., P.G., and J.-O.G. conducted the experiments. G.M., J.K., C.C., and D.C. provided frequency metrology expertise. G.M., D.M.F., B.B., and J.C.C. prepared the initial draft, and all authors critically reviewed and approved the manuscript. D.M.F., A.C., B.B., J.C.C., G.M., V.K., M.C., and K.A.B. analyzed the data. **Competing interests:** A UK priority patent application has been filed in relation to this work. **Data and materials availability:** All data are available at Zenodo (*21*). **License information:** Copyright © 2022 the authors, some rights reserved; exclusive licensee American Association for the Advancement of Science. No claim to original US government works. https://www.science.org/about/science-licenses-journal-article-reuse. This research was funded in whole or in part by the UK Engineering and Physical Sciences Research Council under grant EP/T517884/1. The authors will make the Author Accepted Manuscript (AAM) version available under a CC BY public copyright license.

SUPPLEMENTARY MATERIALS

science.org/doi/10.1126/science.abo1939
Materials and Methods
Supplementary Text
Figs. S1 to S13
References (*22*–*31*)

Submitted 26 January 2022; accepted 11 April 2022
10.1126/science.abo1939

Science

Optical interferometry–based array of seafloor environmental sensors using a transoceanic submarine cable

G. MarraD. M. FairweatherV. KamalovP. GaynorM. CantonoS. MulhollandB. BaptieJ. C. CastellanosG. VagenasJ.-O. GaudronJ. KronjägerI. R. HillM. SchioppoI. Barbeito EdreiraK. A. BurrowsC. ClivatiD. CalonicoA. Curtis

Science, 376 (6595), • DOI: 10.1126/science.abo1939

Relying on repeaters

Underwater optical cables can be used to monitor seismic disturbances and ocean currents, but the signal tends to be integrated over the entire length of the cable, which can be thousands of kilometers long. Marra *et al*. were able to isolate individual segments of a 5800-kilometer-long cable for seafloor monitoring. Because undersea cables have repeaters every 90 kilometers, these segments could each be used as vibrational sensors when coupled with a laser source. This approach allowed the authors to better constrain the location of an earthquake through triangulation, thus offering a method for much better spatial resolution for undersea monitoring. —BG

Science (ISSN) is published by the American Association for the Advancement of Science. 1200 New York Avenue NW, Washington, DC 20005. The title *Science* is a registered trademark of AAAS.